Journal of Thermal Analysis and Calorimetry
https://doi.org/10.1007/s10973-026-15784-x

Probing crystallization of cocoa butter via thermal and X-ray techniques: solving polymorphic transitions using independent components analysis

Hery Mitsutake[1,2,9] · Chris Drakos[2] · Lígia Nunes de Morais Ribeiro[1,3] · Jacob Judas Kain Kirkensgaard[2,4] · Márcia Cristina Breitkreitz[5] · Douglas N. Rutledge[6,7,8] · Eneida de Paula[1] · Heloisa N. Bordallo[2]

Received: 16 December 2025 / Accepted: 28 May 2026

Abstract

Cocoa butter (CB), a natural lipid, is widely used in the food and pharmaceutical industries. However, it is characterized by a polymorphism which significantly affects its physicochemical properties under varying temperatures. Because synthesis, storage and transportation may occur under varying temperatures conditions, understanding its thermal behavior is a crucial step for its characterization and final product quality. In this study, the crystalline structure of CB was analyzed using differential scanning calorimetry (DSC) and small-angle X-ray scattering (SAXS), focusing on developed procedures to isolate form II using variations in heating/cooling rates. DSC curves were deconvoluted using Gaussian curve shapes and the results revealed clear coexistence of polymorphs in the raw material. However, different heating/cooling rates showed different behavior. Recording DSC data with cooling at 10 K min^{-1} affected the crystallization since the crystal memory was not completely erased, while slower rates of 2–5 K min^{-1} allowed more time for crystallization and organization. At these heating rates, it was possible to isolate form II at 14–15 °C. To deconvolute the peaks and trace the polymorphic transitions during the cooling step, the SAXS data were evaluated using independent components analysis (ICA). *In-situ* SAXS provided detailed insight into the crystallization process, demonstrating that the cooling/heating rate and the isotherm time at 0 °C were critical factors. At the same time, ICA helped to isolate signals of the different forms and allowed a direct comparison of different temperature conditions, highlighting the potential of this methodology for characterizing CB and its products.

Keywords Polymorphism · DSC · SAXS · ICA

Introduction

Cocoa butter (CB) is a commodity with increasing importance in recent years. It is best known for its use in the chocolate industry, where it is the main source of triglycerides

Hery Mitsutake and Chris Drakos have contributed equally.

✉ Hery Mitsutake
hemi@build.aau.dk

1 Departamento de Bioquímica E Biologia Tecidual, Instituto de Biologia, Universidade de Campinas - Unicamp, Campinas, SP, Brazil

2 Niels Bohr Institute, University of Copenhagen, Copenhagen, Denmark

3 Institute of Biology, Federal University of Uberlândia, Uberlândia, MG, Brazil

4 Department of Food Science, University of Copenhagen, Copenhagen, Denmark

5 Departamento de Química Analítica, Instituto de Química, Universidade de Campinas – Unicamp, Campinas, SP, Brazil

6 Faculté de Pharmacie, Université Paris-Saclay, Paris, France

7 Muséum National d'Histoire Naturelle, Paris, France

8 Universidade Tecnológica Federal Do Paraná, Curitiba, Brazil

9 Present Address: Department of the Built Environment, Aalborg University, Thomas Manns Vej 23, 9220 Aalborg East, Denmark

Published online: 02 July 2026

(TAG) [1]. It is also used in the pharmaceutical and cosmetic industries as a natural excipient. It serves as the main component in the core of lipid-based nanoparticles, where active pharmaceutical ingredients are dissolved to enhance drug delivery efficiency [2–4]. Another function of CB is to mask unpleasant taste and flavor defects, making the pharmaceutical products more palatable to patients. Soddu et al. developed solid lipid nanoparticles using CB as the solid lipid and obtained particle sizes around 390–600 nm which were stable for one month [5]. Our group also developed a CB-based nanostructured lipid carrier to encapsulate lidocaine which was stable for over one year [6]. Nevertheless, dealing with CB is not easy due to its polymorphism, the effect of temperature on this property, and the variations of its market value [7].

CB, derived from the *Theobroma cacao* plant, consists predominantly of three TAGs, which constitute up to 80% of the total TAGs: 1,3-dipalmitoyl-2-oleoyl-sn-glycerol (POP), 1-palmitoyl-2-oleoyl-3-stearoyl-sn-glycerol (POS), and 1,3-distearoyl-2-oleoyl-sn-glycerol (SOS). Studies suggest that interactions between POS, POP, and SOS influence CB polymorphism [8–10], that is, its ability to exist in multiple crystalline phases. Controlling polymorphism is critical in the pharmaceutical industry, as different polymorphs exhibit distinct physical properties. Wille and Lutton found six different polymorphs of CB, with the melting points of forms I, II, III, IV, V, and VI being 17.3, 23.3, 25.5, 27.5, 33.8, and 36.3 °C, respectively [11]. However, van Malssen et al. suggested that forms V and VI are subphases of a triclinic form [11, 12]. According to them, some polymorphs are probably nonhomogeneous crystalline states—form VI being the result of a phase separation, not a real polymorphic form. The polymorphism of CB is highly affected by differences in temperature. Form II can be found below 18 ºC but not at room temperature, where it tends to change into forms III or IV. This means that form II can be formed if formulations are stored in a fridge or submitted to an ice bath or put in the luggage compartment of a plane. In this sense, understanding CB polymorphic transitions at different temperature variation rates is relevant for making more reproducible CB products and guaranteeing the quality during storage and transportation.

The most common techniques to characterize CB polymorphism are X-ray diffraction [8, 11–13] and differential scanning calorimetry (DSC) [4, 13, 14], but other methods have brought new insight. For instance, Bresson et al. used Raman spectroscopy to differentiate the polymorphic forms and liquid phase of CB [15]. The carbonyl region (1780–1700 cm^{-1}) showed changes such as shifts in position and new bands after cooling procedure. This happened also for other vibrations related to skeletal modes, C–H and unsaturated bonds. Additionally, Reinke et al. used small-angle X-ray scattering (SAXS) to follow the migration of lipids during chocolate blooming, i.e., the formation of white defects on the chocolate surface [16], while MacMillan and Roberts studied the temperature effect using SAXS on polymorphic forms III and IV, simulating industrial tempering processes, where the effect of sheared samples is highlighted [17]. Furthermore, MacMillan et al. showed that polymorph III is the initial nucleating phase during the tempering process using wide-angle X-ray scattering (WAXS) [18]. The effect of milk fat alternatives (MFA) in vegan chocolate was evaluated by Fiore et al. using SAXS and WAXS, where the addition of MFA changed the CB polymorph detected at room temperature, showing its influence on kinetic transformations [1].

Considering all the difficulties in maintaining a single polymorphic form throughout the shelf-life time of cocoa butter, since temperatures variations and/or minor compounds influence its crystallization behavior and polymorphic stability, a detailed understanding of its thermal and structural transitions is essential for ensuring reproducibility and product quality. Although DSC and X-ray scattering techniques have previously been used to characterize cocoa butter polymorphism, resolving overlapping polymorphic transitions during dynamic crystallization remains challenging due to the coexistence of multiple crystalline forms and partially ordered states. In the present study, DSC and SAXS combined to analyze cocoa butter crystallization under different heating and cooling rates. To deal with the complexity of the data, independent components analysis (ICA) was used to deconvolute the SAXS datasets by extracting the underlying source signals and the related polymorphic transitions during the cooling step at slow, intermediate and fast rates. ICA was chosen because it can be used as a batch process monitoring tool to deconvolve the source signals/pure signals from the data and has no problem dealing with rotational ambiguity [19, 20]. Rotational ambiguity is a problem that is encountered during bilinear decomposition, where different linear combinations can give equivalent responses.

Materials and methods

Materials

Cocoa butter (CB), CAS number 8002–31–1, was purchased from Engetec Engenharia das Essências (São Paulo, Brazil). This sample was heated and cooled at different temperature variation rates, and with different initial and final temperatures.

Differential scanning calorimetry (DSC)

DSC measurements were carried out on CB using a DSC 214 Polyma apparatus (Netzsch, Germany). The temperature

was calibrated using an Indium standard. Samples with similar masses of around 3 mg were sealed in aluminum crucibles in a closed system and measured between approximately 0–60 °C under a liquid N_2 atmosphere. The sample chamber was purged with N_2 gas at 40 mL min^{-1}, while a protective gas flow of 60 mL min^{-1} N_2 was used. Before the experiment, the DSC signal was measured with empty reference and sample crucibles to correct the baseline.

Table 1 summarizes the CB heating and cooling procedures chosen, based on Bresson's work to isolate form II [15], with slight modifications in the conditions. These temperatures are also common in the synthesis of nanoparticles, where the excipients are heated up to around 10–15 ºC above their melting points and cooled using ice or water baths [21, 22]. The measurements were done in duplicate to verify reproducibility between runs. Because the melting and solidification temperatures of the different CB polymorphs are very close, the DSC curves typically show multiple overlapping peaks. These appear as broad peaks and/or peak shoulders instead of narrow peaks. Therefore, curve deconvolution of the DSC datasets was used to identify hidden peaks. To do this deconvolution, the Fraser-Suzuki function was applied to the DSC curves using Origin Pro 2020 and Peak Deconvolution v. 2.21. The number of peaks and their initial positions were estimated by applying second derivative on DSC curves. The maximum number of iterations was 200 and chi-tolerance of 10^{-6} was applied as a stopping criterion.

Small- and wide-angle X-ray scattering (SWAXS)

The SWAXS data were obtained using a Nano-inXider (Xenocs) equipped with a 30 W microfocus sealed Cu-tube producing X-rays with a wavelength of 1.54 Å. The windowless beam path is under vacuum to the detectors for low-noise, high-signal measurements. The system is equipped with two detectors allowing simultaneous detection of the full momentum transfer, or q-range from 0.01 to 4.24 $Å^{-1}$. The two detectors are q-calibrated using silver behenate (SAXS) and NIST Certified Reference Material 660a (LaB_6) (WAXS), respectively. A copper cell was employed to guarantee proper heat flow, and a Peltier stage for temperature control (HFSX350, Linkam scientific instruments Ltd., Surrey, United Kingdom). The sample was maintained at 60 ºC for one hour and afterward cooled at 2, 5 or 10 K min^{-1} until 0 ºC, simulating the procedure used in the DSC analysis with scattering data recorded continuously in 60s intervals. The sample is sealed between 5–7 µm thick mica windows, and an empty cell measurement was used for background correction. The mica mostly gives rise to a low flat background in the WAXS region but does present occasional isolated Bragg reflections which are manually masked out before radial averaging. These data were exported in '.dat' format and analyzed using Matlab v. 24.2. The spectra were obtained in q ($Å^{-1}$), and were then converted to d-spacing (Å) using Eq. 1 [23]:

Table 1 Temperature program used for DSC experiments on CB

Step	Experiment 1	Experiment 2	Experiment 3
1	Memory erase Heating 2 K min^{-1} Temperature range: 27–60 ºC Hold temperature at 60 ºC for 10 min	Memory erase Heating 5 K min^{-1} Temperature range: 27–60 ºC Hold temperature at 60 ºC for 10 min	Memory erase Heating 10 K min^{-1} Temperature range: 27–60 ºC Hold temperature at 60 ºC for 10 min
2	Cooling 2 K min^{-1} Temperature range: 60–0 ºC Hold temperature at 0 ºC for 60 min	Cooling 5 K min^{-1} Temperature range: 60–0 ºC Hold temperature at 0 ºC for 60 min	Cooling 10 K min^{-1} Temperature range: 60–0 ºC Hold temperature at 0 ºC for 60 min
3	Memory erase Heating 2 K min^{-1} Temperature range: 0–60 ºC Hold temperature at 60 ºC for 10 min	Memory erase Heating 5 K min^{-1} Temperature range: 0–60 ºC Hold temperature at 60 ºC for 10 min	Memory erase Heating 10 K min^{-1} Temperature range: 0–60 ºC Hold temperature at 60 ºC for 10 min
4	Cooling 2 K min^{-1} Temperature range: 60–0 ºC Hold temperature at 0 ºC for 60 min	Cooling 5 K min^{-1} Temperature range: 60–0 ºC Hold temperature at 0 ºC for 60 min	Cooling 10 K min^{-1} Temperature range: 60–0 ºC Hold temperature at 0 ºC for 60 min
5	Memory erase Heating 2 K min^{-1} Temperature range: 0–60 ºC Hold temperature at 60 ºC for 10 min	Memory erase Heating 5 K min^{-1} Temperature range: 0–60 ºC Hold temperature at 60 ºC for 10 min	Memory erase Heating 10 K min^{-1} Temperature range: 0–60 ºC Hold temperature at 60 ºC for 10 min
6	Cooling 2 K min^{-1} Temperature range: 60–0 ºC Hold temperature at 0 ºC for 60 min	Cooling 5 K min^{-1} Temperature range: 60–0 ºC Hold temperature at 0 ºC for 60 min	Cooling 10 K min^{-1} Temperature range: 60–0 ºC Hold temperature at 0 ºC for 60 min

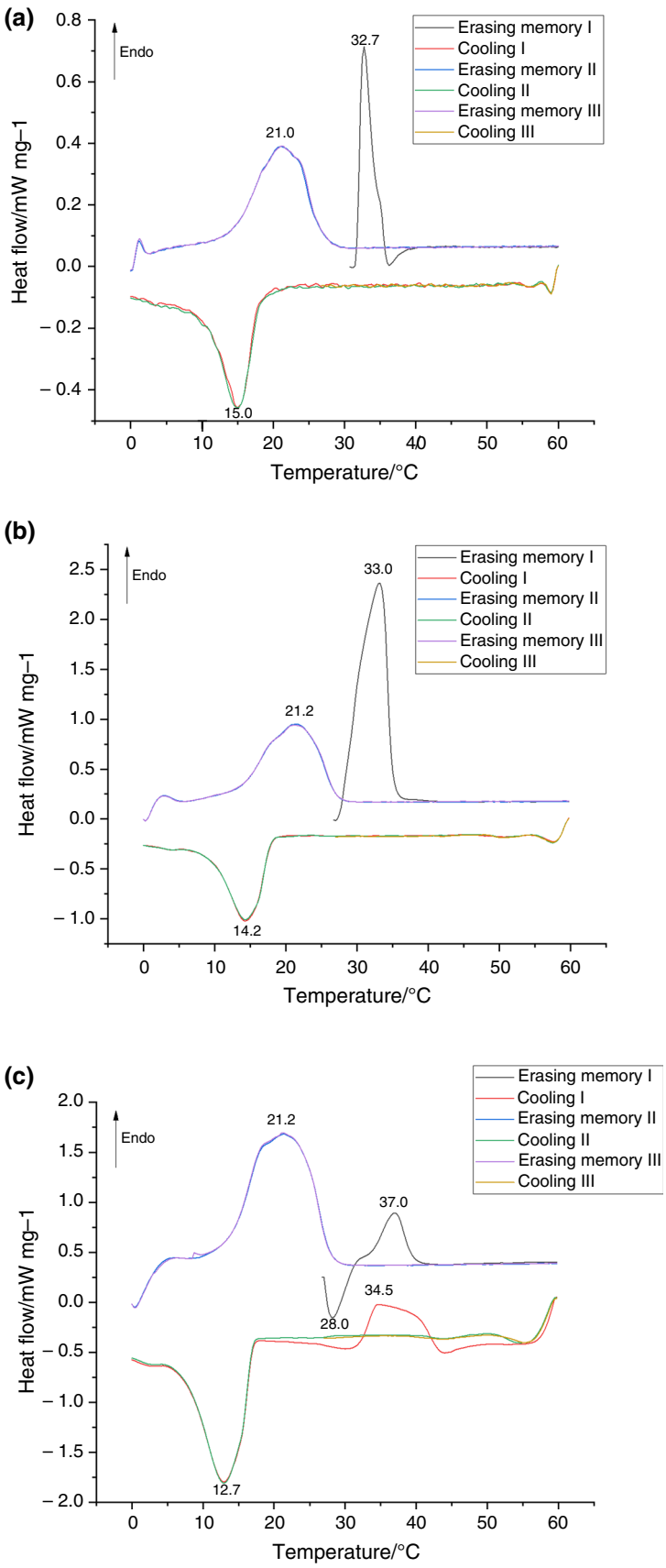

Fig. 1 DSC curves obtained during experiments performed at: **a** 2 K min^{-1}, **b** 5 K min^{-1} and **c** 10 K min^{-1}

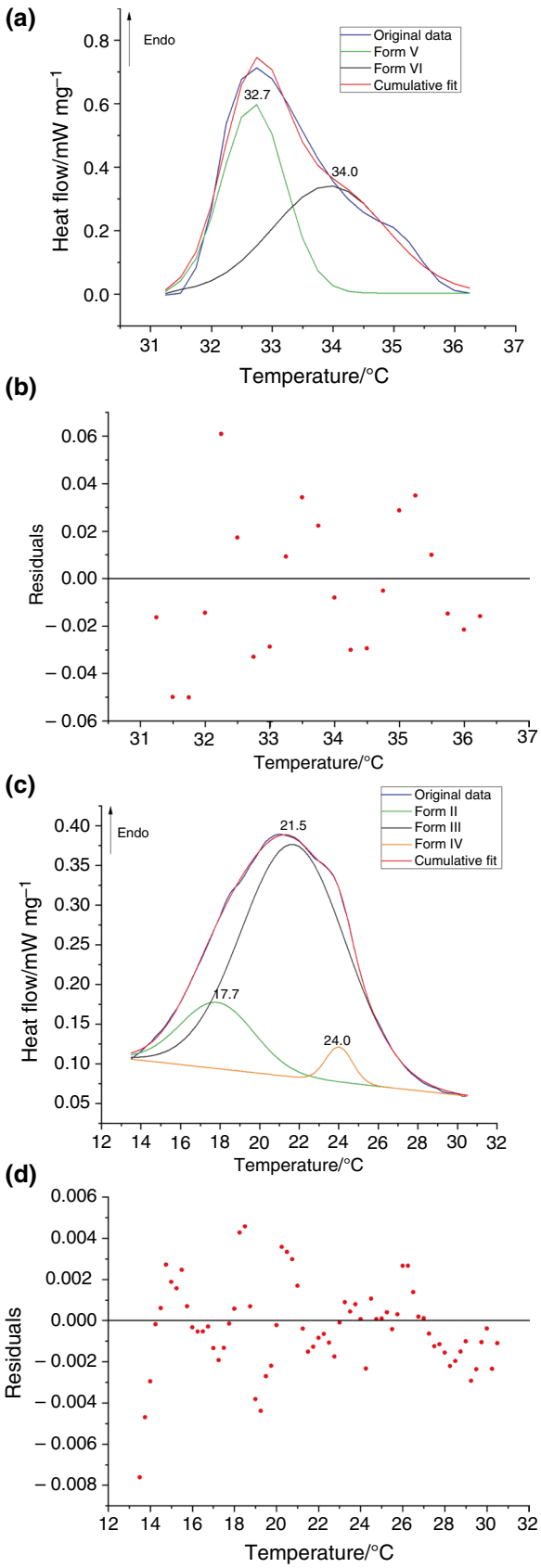

Fig. 2 Deconvolution of DSC curves obtained during the crystal-memory erasing step at 2 K min^{-1}: **a** fitted curve, **b** residuals of the fitted curve, **c** deconvolution of the second heating step, and **d** corresponding residuals. The fitted contributions indicate coexistence of multiple polymorphic forms in the raw material and the formation of metastable polymorphs during reheating

$$d = \frac{2\pi}{q} \tag{1}$$

The main peaks of CB are in the range of 30.0–78.0 Å and so our analysis focused on this region. The full q-range measurements confirm that no relevant peaks are present outside this range as shown in Fig. S1. Independent components analysis (ICA) was used to extract the source signals (***S***) and their proportions (***A***) from the matrix (***X***) composed of the observed SAXS spectra obtained from all experiments. The process is based on Eq. 2 [19, 24]:

$$\boldsymbol{X} = \boldsymbol{A}\boldsymbol{S}^{\mathrm{T}} \tag{2}$$

where the superscript "*T*" indicates that ***S*** is transposed. The Joint Approximate Diagonalization of Eigenmatrices (JADE) algorithm was chosen for this application. It calculates linear transformations of the original observed signals to maximize the statistical independence of the source signals in ***S*** [24]. The number of components was determined using the ICA-by-Blocks function [25]. ICA was done using Matlab v. 24.2, after baseline correction using the rubber band method available in IRootLab [26].

Results and discussion

DSC results

Figure 1 shows the DSC curves obtained for the three experiments. While 2–5 K min^{-1} have the same melting point in the original material (step erasing memory I), 10 K min^{-1} showed a different behavior. It has an exothermic phenomenon at 28.0ºC, and the melting temperature was 37.0ºC. This can indicate that at higher heating rates there is a new rearrangement of CB crystals at 28.0ºC (the exothermic event) that generates more stable polymorphs, with melting point of 37.0ºC which was at around 33 ºC in the other conditions. Further discussion about these different kinetics will be given after presentation of the deconvolution of DSC curves.

Figure 2a shows the deconvolution of the DSC curve obtained during heating at 2 K min^{-1} rate in Experiment 1 (Table 1) where more than one polymorph can be found. Curve deconvolution was applied and there are two polymorphs in the initial state: forms V and VI with melting points at 32.7–34.0 °C, respectively. Thus, it was possible

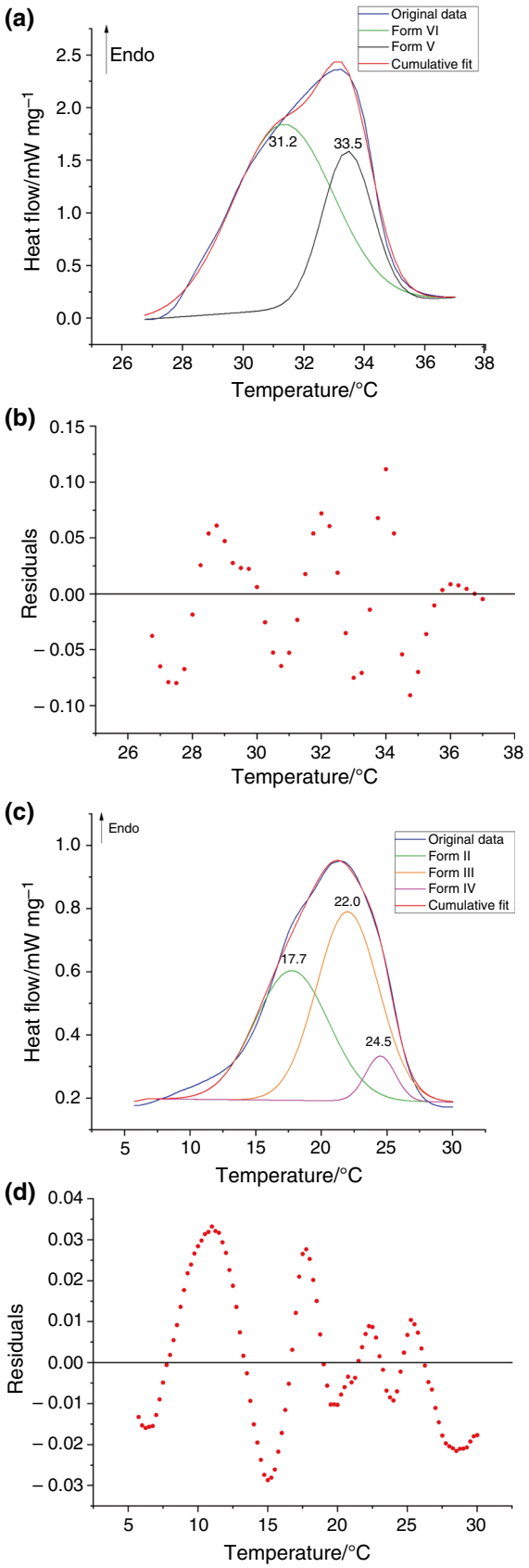

Fig. 3 Deconvolution of DSC curves obtained during the crystal-memory erasing step at 5 K min^{-1}: **a** fitted curve, **b** residuals of the fitted curve, **c** deconvolution of the second heating step, and **d** corresponding residuals. The thermal behavior demonstrates the influence of intermediate heating and cooling rates on polymorphic transitions and crystallization pathways

to verify that there are at least two different polymorphs in the raw material, confirming the importance of erasing the crystal memory [11, 12, 15]. Figure 1a shows the first and second cooling processes where it was possible to isolate the metastable form II following the protocol proposed by Bresson [15]. The procedure was reproducible, with a solidification point equal to 15.0 ºC. Also, the narrower peak confirmed the presence of only form II. Additionally, as expected, forms III and IV were also produced (Fig. 2c) during heating. However, this also implies that strict temperature control is crucial to avoid polymorphic transitions and ensure reproducibility/quality.

The deconvolution of the DSC curve obtained during the memory erasing step at 5 K min^{-1} rate in Experiment 2 (Table 1) indicated again the presence of two polymorphs (Fig. 3a). The melting point of the main structure was at 31.2 ºC, corresponding to form V, while the second contribution originates from form VI with melting point at 33.5 ºC. During the cooling steps at 5 K min^{-1}, only form II was formed with solidification point at 14.2 ºC (Fig. 1b) while forms II, III and IV are also produced during the heating process (Fig. 3c).

Figure 4a shows the DSC curve obtained during the memory erasing step at 10 K min^{-1} rate in Experiment 3 (Table 1) which is different from that observed at the slower heating rates (Figs. 2a and 3a), where the main polymorph was form V; at this heating rate, the melting point was at 37.0 ºC, corresponding to form VI. The first and second cooling at 10 K min^{-1} (Fig. 1c) gave a form I crystal where the main solidification point was at 12.7 ºC. However, the broader peak also suggested the presence of more than one polymorph. The Fraiser-Suzuki function from Peak Deconvolution does not work for negative peaks, so the second derivative was applied on the first crystallization step. The first event was found at 34.2 ºC (Fig. 4b) and did not happen when using slower temperature variation rates (Figs. 2b and 3b) or the other crystallization steps at 10 K min^{-1}. This indicated that some of the crystals had not completely melted, due to the high heating rate, and so the crystal memory was not fully erased. The second event happened at 17.0 ºC, which is the onset temperature of CB crystallization. Due to the fast cooling rate, a less stable polymorph could be formed at 15.7 ºC while the main crystallization of Form I happens at 13.0 ºC. Ideally, the residuals are random. However, the polymorphic transitions of CB during the heating and cooling produce overlapping peaks in the

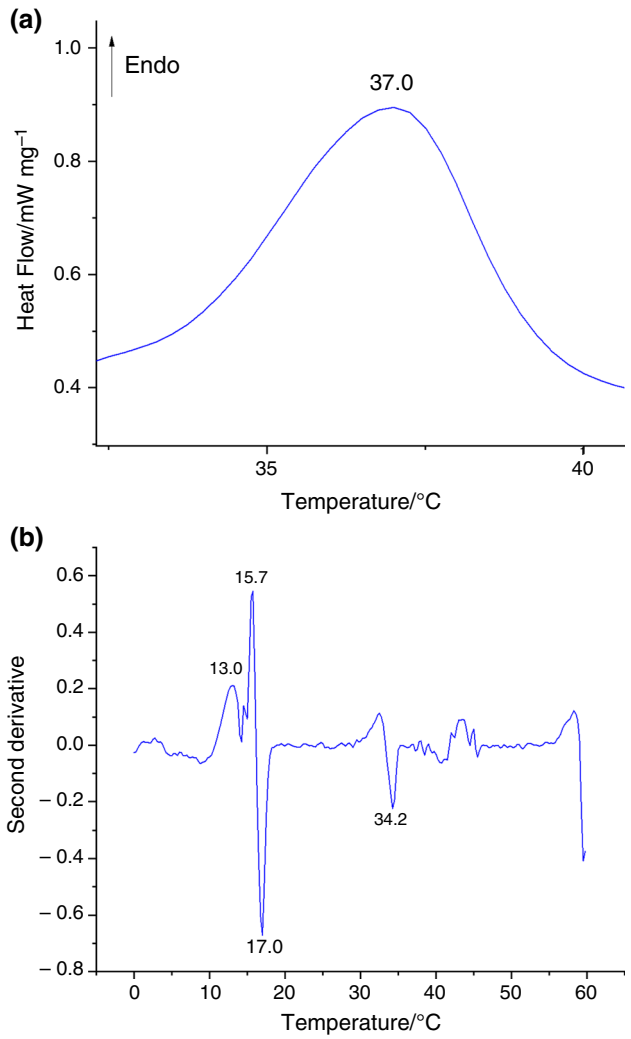

Fig. 4 DSC analysis obtained at 10 K min^{-1}: **a** curve recorded during the crystal-memory erasing step and **b** second derivative of the first cooling step. The additional thermal event observed at high heating rate suggests incomplete crystal-memory erasure and formation of metastable polymorphic structures

deconvolution. This is indicative of more complex processes and did not give random residual in Figs. 2b, 2d, 3b and 3d.

To summarize, experiments 1 to 3 were based on the methodology proposed by Bresson to isolate form II [15]. Experiment 1 is very similar to the proposed design but includes a longer duration for the memory-erasing step. Experiments 2 and 3 included changes in the temperature rates. The high heat flow, 10 K min^{-1}, favored form I instead of form II as the main polymorph and required more time at the isotherm of 60 ºC, or otherwise two heating cycles, to completely erase the crystal memory. On the other hand, using cooling rates of 2–5 K min^{-1} generated form II. From these results, it can be concluded that the heating rate is as crucial as the final temperature and isotherm time to erase CB crystal memory. However, this parameter is often overlooked in the literature [12, 14, 27]. Moreover, CB exhibits complex polymorphism at room temperature, where multiple crystalline forms often coexist due to slow polymorphic transitions; therefore, different polymorphs may already be present in the raw material, as demonstrated by the first step in all our experiments. This implies that, during the synthesis of CB-based nanoparticles, it is highly recommended to use 60 ºC as the final temperature, instead of just 10–15 ºC above of its melting point (around 33–36 ºC, if we consider form VI as the main one). Using this pre-step can also help make this process more reproducible, as demonstrated by the heating steps during these experiments.

X-Ray scattering results

While DSC provided information about thermal transitions and crystallization kinetics, SAXS enabled direct monitoring of lamellar structural evolution during cooling by revealing structural changes associated with the observed polymorphic transitions. Figure 5 shows SAXS patterns obtained during the three experiments carried out when cooling between 60 and 0 ºC. As shown in DSC (Fig. 1), the fast-cooling rate (10 K min^{-1}) did not produce Form II, but the metastable Form I and had problems during the crystallization since not enough time was given for the reorganization of CB triacylglycerols. In SAXS, this was also observed by the lower intensities in these conditions.

Using a cooling rate of 2 K min^{-1}, the first reflection was observed at 49.5 Å while a second at 54.2 Å was detected at temperatures below 10.4 ºC. These long-spaced values are similar to values found for the polymorphic form β' family [13]. The crystallization process is very different when the cooling rate is 5 K min^{-1} where the main reflection is at 50.9 Å, but with a broader shoulder. This is indicative of a more amorphous phase. Besides this, a new reflection is formed at 53.5 Å suggesting a new lamellar reorganization during the cooling step. Using a fast-cooling rate, 10 K min^{-1}, the reflection at 49.7 Å appeared around 18 ºC. This is a higher temperature when compared with the 2–5 K min^{-1} rates; both started the crystallization around 12 ºC. However, at 0 ºC, different lamellar distances were found when a fast-cooling rate was employed. The sharper and more intense reflections formed at very slow cooling indicated that a more crystalline structure was obtained than in other cases. These results corroborate the DSC findings indicating an issue with crystal memory. Specifically, when a cooling rate of 10 K min^{-1} is used, the presence of residual crystals in the first run and the broader DSC curves suggest incomplete erasure. The assignment of reflections to specific polymorphic forms was based on the combined interpretation of SAXS profiles, DSC transitions, and literature-reported d-spacing values. Table 2 shows the onset temperature for each technique for the crystallization step. While

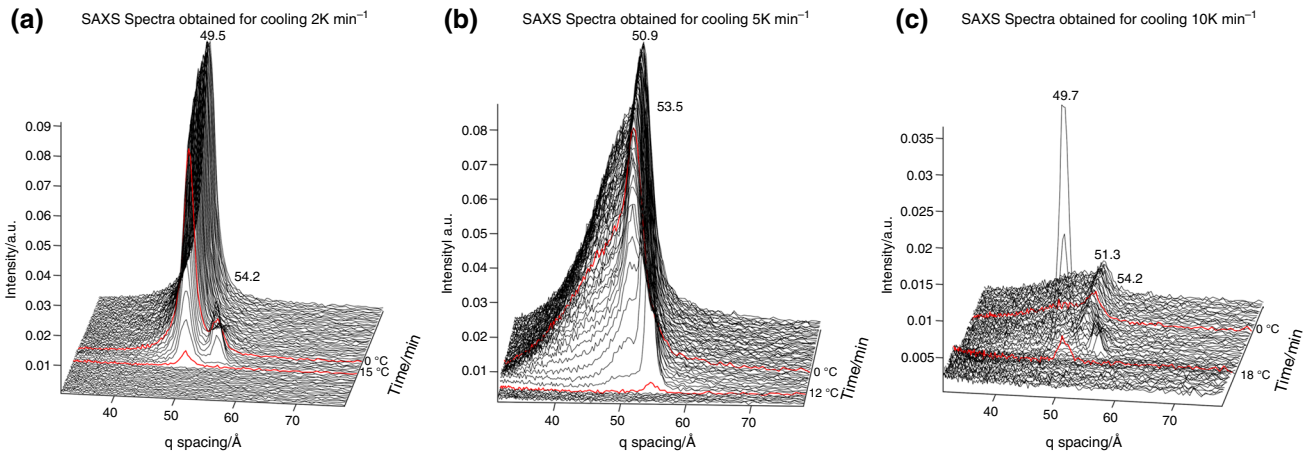

Fig. 5 In situ SAXS patterns of cocoa butter recorded during cooling from 60 to 0 °C using: **a** 2 K min^{-1}, **b** 5 K min^{-1}, and **c** 10 K min^{-1}. Variations in reflection intensity, width, and d-spacing reveal differences in lamellar organization and polymorphic evolution as a function of cooling rate

Table 2 Onset temperatures for crystallization obtained in DSC and SAXS for CB

Experiment	Technique	Onset temperature of crystallization /ºC
1 (2 K min^{-1})	DSC–1st cooling	20.24
	DSC–2nd cooling	21.24
	SAXS	15
2 (5 K min^{-1})	DSC–1st cooling	20.00
	DSC–2nd cooling	19.00
	SAXS	12
3 (10 K min^{-1})	DSC–1st cooling	18.25
	DSC–2nd cooling	17.75
	SAXS	18

it is the same in the highest tested temperature rate–around 18ºC, there is a difference of 6–8ºC comparing DSC and SAXS. Rigolle et al. suggested that before the formation of the lamellar structure there is a nucleation step [28]. The first phenomenon can be detected by DSC, whereas SAXS requires the formation of more organized lamellar structures. This also explains why at 10 K min^{-1} the onset temperatures in both techniques are the same: the two steps are happening at the same time; however, the crystals are not well formed when compared with the slower case, as 2 K min^{-1}.

As mentioned in Sect. "Small- and Wide-angle X-ray Scattering (SWAXS)"., ICA-by-Blocks was used to determine that five ICs were required to describe the system (Figure S2). Figures 6a and 7a show the results for the first independent component (IC1) of the SAXS dataset. Although negative SAXS intensities are not physically possible, the JADE algorithm employed to do the ICA-based bilinear decomposition does not use non-negativity constraints. Consequently, small negative signals may appear. However, the negative values found here are low in intensity and likely related to baseline shifts or noise. Importantly, the positions identified in each IC correspond to reflections from the original SAXS profiles (Fig. 5). Figure 6 presents the source signals, extracted from the observed signals while the proportions in Fig. 7 show how these signals evolve during cooling. For example, there are three reflections in IC2 (Fig. 6b) at 49.4, 50.9 and 53.4 Å. This indicates that these reflections are statistically dependent and, the corresponding proportions plot (Fig. 7b), shows no changes until about 20 ºC, after which they increase together in intensity down to l0 ºC.

The reflection at 49.4 Å (Fig. 6a) is consistent with reported d-spacing values for form II, indicating that IC1 corresponds is predominantly associated with this polymorph [13]. Observing the proportions (Fig. 7a), at 2 K min^{-1}, this polymorph begins to form at 14.9 ºC and slowly increases until 0 ºC. At 5 K min^{-1}, although this process begins at similar temperature, the relative amount of form II is lower throughout cooling (Fig. 6a). However, the abundance of this form increases during the isotherm hold at 0 ºC. On the other hand, at 10 K min^{-1}, this polymorphic form appears at a higher temperature (17.2 ºC) but disappears below 10.0 ºC (Fig. 7a). The most important reflection for IC2 is the broad peak at 47.2 Å (Fig. 6b). It can be related

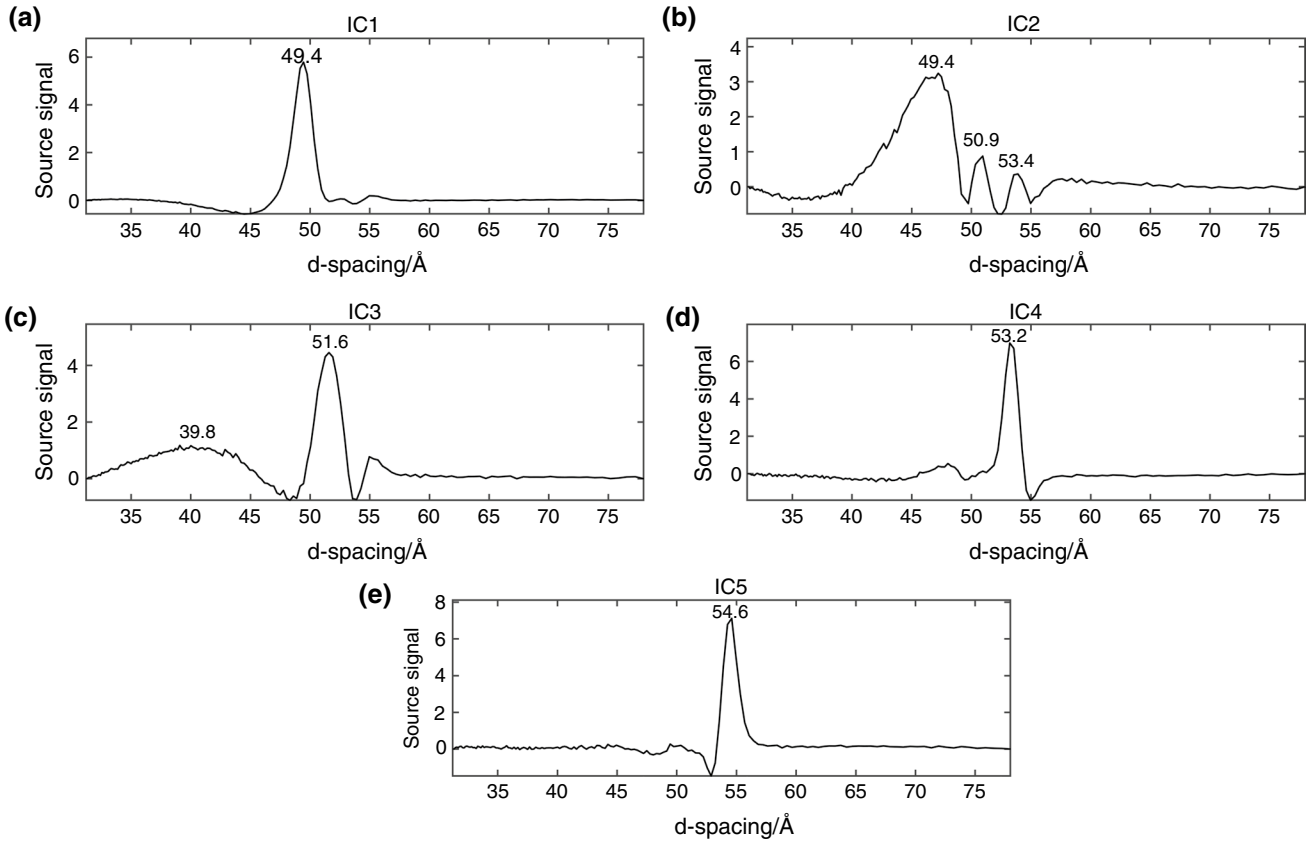

Fig. 6 Independent components (ICs) extracted from SAXS datasets using ICA: **a** IC1, **b** IC2, **c** IC3, **d** IC4, and **e** IC5. The components represent statistically independent structural contributions associated with different polymorphic states and partially ordered phases during cocoa butter crystallization

to metastable forms, disordered regions or even liquid phases [12, 13]. The additional reflections at 50.9–53.4 Å (Fig. 6b) are consistent with reflections previously attributed to form II and form I [13, 17]. The behavior of IC2 is similar to that of IC1 (Fig. 7a), indicating coexistence of form II with another polymorph, together with amorphous phase or partially ordered phase (Fig. 7b). The amorphous phase differs from the remaining liquid phase since it retains some degree of structural organization and may therefore be considered a "liquid–crystal" state [13]. However, when comparing cooling rates, this component is the most prominent in Experiment 2 (5 K min^{-1}). This suggests that intermediate cooling rates require longer isotherm holding at 0ºC for complete crystallization into form II. IC3 is very similar to IC2 (Fig. 7c), suggesting coexistence of related polymorphic contributions with similar kinetic behavior. Nevertheless, its most intense reflection occurs at 51.6 Å and which is consistent with reported values for form III (Fig. 7c). Reflections consistent with the more stable forms V or VI appear below 10 ºC, mainly at 5 K min^{-1}, as indicated by IC4 (Figs. 6d and 7d). However, the relative contributions of these reflections decrease during the isothermal step at 0 °C, while signals associated with forms I and II become more prominent. This phenomenon occurs only at low and intermediate heating rates (2–5 K min^{-1}). Similar behavior is observed for IC5, whose dominant reflection is consistent with reported values for form VI (Fig. 6e and 7e). Even though forms V and VI are known to be stable, maintaining the sample for a longer time at 0 ºC can induce the formation of states such as form II and III.

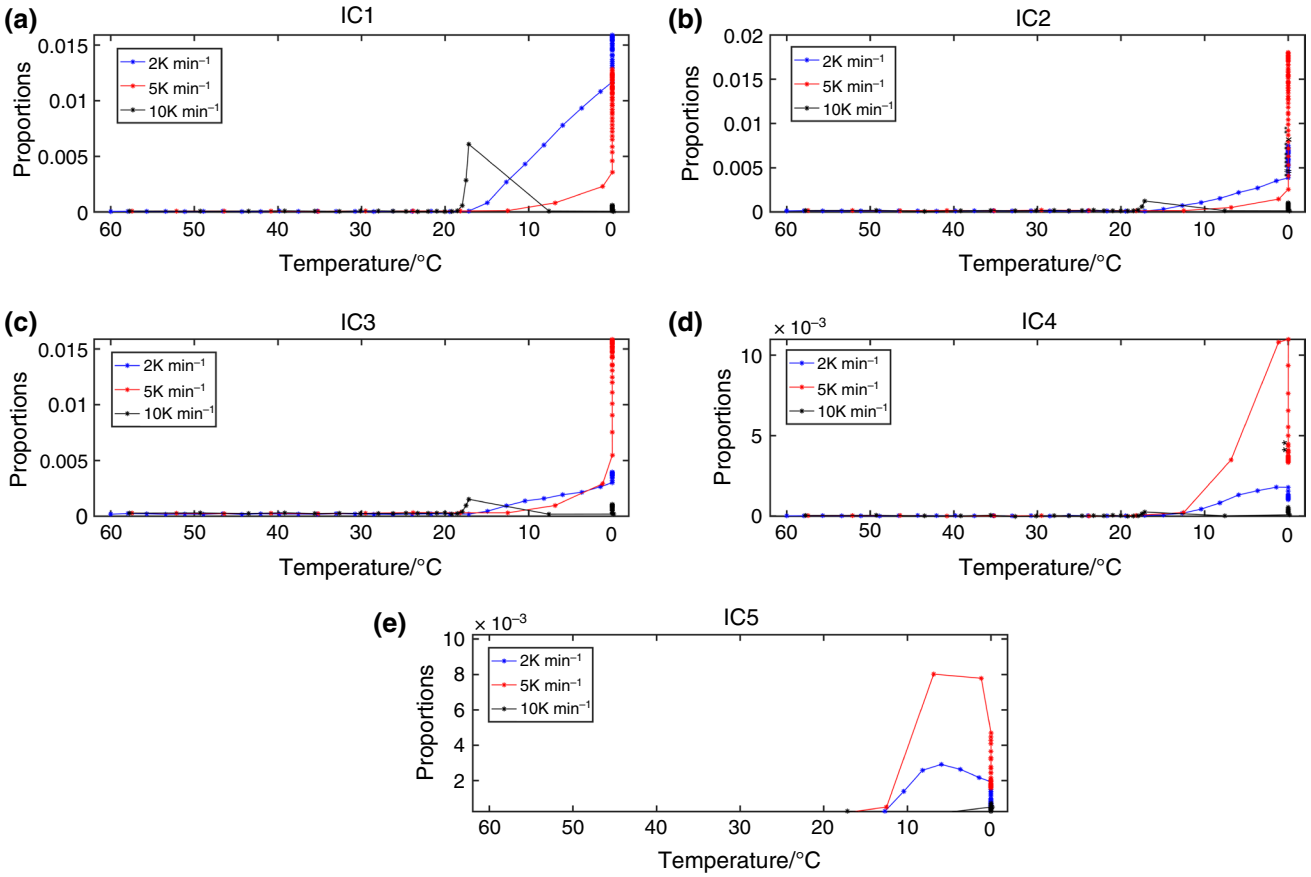

Fig. 7 Relative proportions of the independent components obtained from ICA during cooling experiments: **a** IC1, **b** IC2, **c** IC3, **d** IC4, and **e** IC5. The evolution of component intensities illustrates the temperature-dependent competition among polymorphic forms and disordered structural states under different cooling conditions

Multiple polymorphic forms coexist in CB, with Bragg reflections observed in the SAXS data that are often closely spaced or partially overlapping. In addition, peak broadening can arise from lamellar structural disorder and thermal fluctuations. These conditions do not satisfy the assumptions required for a reliable Scherrer analysis, which attributes peak broadening primarily to finite crystallite size [29, 30]. Although ICA can help separate overlapping signals, it produces statistically independent components rather than true isolated single-phase reflections [31]. Consequently, applying the Scherrer equation to ICA-resolved peaks may still not yield meaningful crystallite-size estimates. For this reason, we focused instead on the evolution of d-spacing, which provides a more robust measure of lamellar structural changes. The ICs obtained in this model were not dominated by noise, and their peaks correspond to real reflections of CB polymorphic forms. The residual plot is shown in Fig. S3 further corroborates that these components are not mathematical artifacts or products of noise-fitting. Figure 8 summarizes the experimental conditions and the main findings obtained in this work.

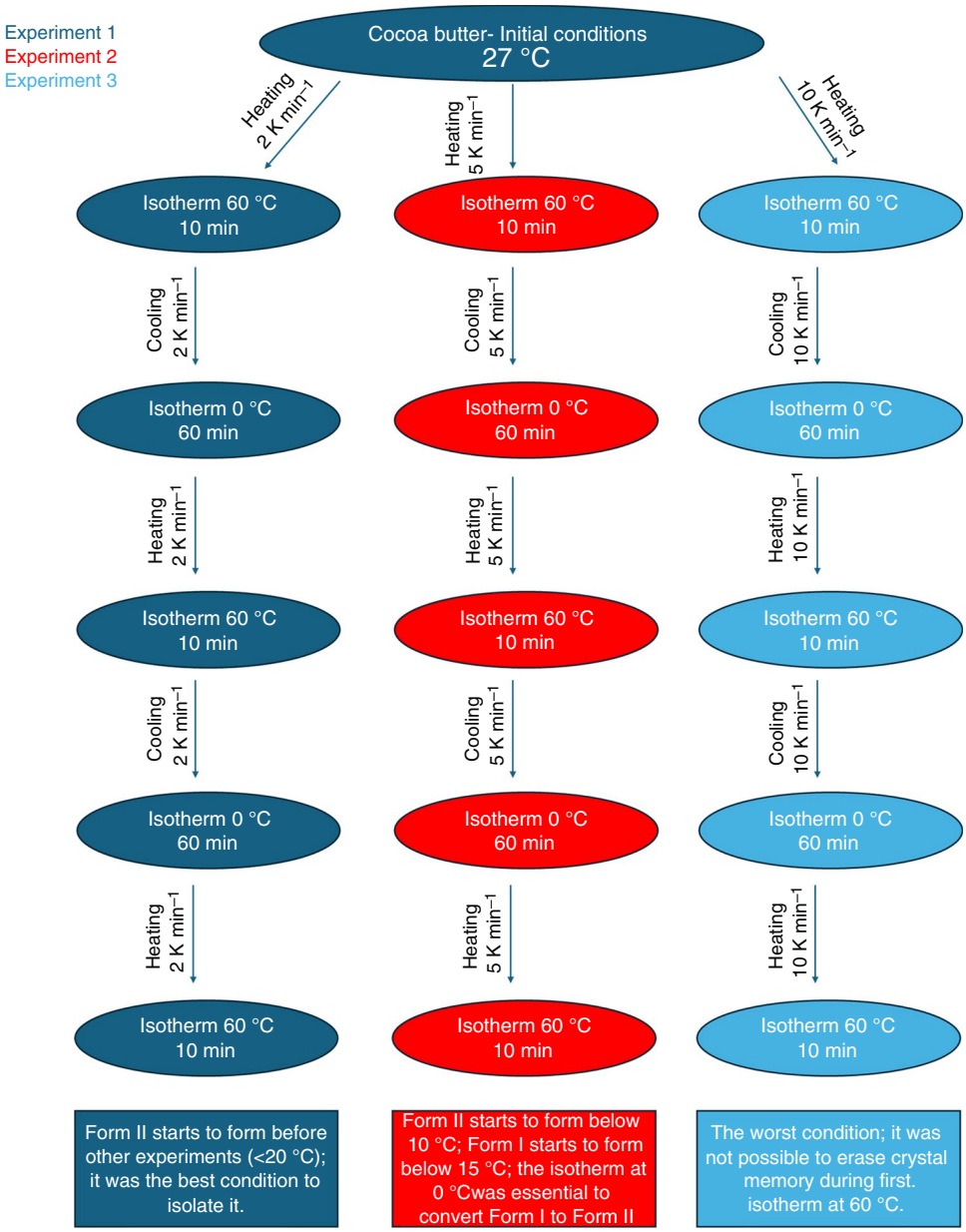

Fig. 8 Schematic summary of the experimental conditions and the main polymorphic behaviors observed during cocoa butter crystallization at different heating and cooling rates. Slow thermal rates promoted formation of more ordered form II structures, whereas fast rates favored metastable and partially ordered phases

Conclusions

The combined DSC and SAXS analyses provided for a detailed understanding of cocoa butter (CB) crystallization across varying cooling rates, revealing how polymorphic transformations progress from initial nucleation to final lamellar organization. DSC showed the coexistence of multiple polymorphic forms in the raw material and demonstrated that successful crystal memory erasure is highly dependent on heating rate. Rapid heating at 10 K min^{-1} failed to fully eliminate residual crystalline domains, which subsequently redirected crystallization pathways, whereas slower heating rates (2–5 K min^{-1}) effectively erased prior structural memory, enabling reproducible crystallization of the desirable form II polymorph.

SAXS provided direct structural evidence of how cooling kinetics governs lamellar development. Slow cooling (2 K min^{-1}) promoted the formation of sharp, intense reflections characteristic of highly organized β′-type lamellae, indicative of superior structural order. Intermediate cooling (5 K min^{-1}) favored a more complex microstructure, where ordered crystalline domains coexisted with partially disordered or transitional phases. In contrast, fast cooling (10 K min^{-1}) produced weak, diffuse reflections associated with poorly developed lamellae, corroborating DSC findings that rapid cooling encourages incomplete melting and stabilization of metastable structures.

ICA further added to the SAXS interpretation by resolving complex overlapping reflections into five statistically

independent structural components, each representing distinct polymorphic states and kinetic pathways. IC1 followed the progressive emergence of form II, while IC2 and IC3 exposed the dynamic competition among disordered domains and metastable forms I–III. IC4 and IC5 captured the transient formation of more stable β-family polymorphs (V/VI), highlighting their temporary role before conversion under low-temperature holding conditions. The ICA proportion profiles clearly demonstrated that slow cooling steadily favors form II, intermediate cooling intensifies polymorphic competition, and fast cooling largely suppresses stable lamellar development. The observed agreement between ICA-resolved reflections and experimental SAXS profiles, combined with minimal residuals, confirms that ICA successfully extracted physically meaningful structural information.

Collectively, these findings establish that CB crystallization is controlled by a highly sensitive interplay among thermal history, kinetic barriers, and polymorphic competition. Controlled slow cooling optimizes the formation of structurally ordered form II, while accelerated cooling shifts the system toward metastable, disordered, or kinetically trapped states. By integrating DSC, SAXS, and ICA, this work provides a powerful multidimensional framework for decoding complex polymorphic behavior in lipid systems. Beyond cocoa butter, this methodology offers broad industrial relevance for designing processing strategies that precisely control crystalline structure, thereby improving product stability, texture, and storage performance in CB-based and related materials.

Supplementary Information The online version contains supplementary material available at https://doi.org/10.1007/s10973-026-15784-x.

Acknowledgements The authors thank São Paulo Research Foundation (FAPESP 21/07224-8 – H.M. fellowship), Conselho Nacional de Desenvolvimento Científico e Tecnológico (CNPq—E.P fellowship), Coordenação de Aperfeiçoamento de Pessoal de Nível Superior (CAPES, Finance Code 001) and Carlsberg Foundation (H.N.B. grant 2013_01_0589 and CF19-0521) for financial support. SAXS data was generated via a research infrastructure at University of Copenhagen, partly funded by FOODHAY (Food and Health Open Innovation Laboratory, Danish Roadmap for Research Infrastructure).This work was supported by the Danish Agency for Higher Education and Science (ESS Lighthouse: Colloids and Interfaces in Food and Pharma; Grant No. 726510).

Author contributions HM: data curation, formal analysis, investigation, validation, visualization, writing—original draft. CD: formal analysis, investigation, validation, writing—review & editing. LNMR: formal analysis, software, validation, visualization, writing—original draft, writing—review & editing. JJKK: formal analysis, investigation, writing—review & editing. MCB: conceptualization, supervision, writing—review & editing. DNR: conceptualization, methodology, software, supervision, validation, writing—review & editing. EP: conceptualization, funding acquisition, methodology, project administration, resources, supervision, writing—review & editing. HNB: formal analysis, funding acquisition, methodology, project administration, resources, supervision, writing—review & editing.

Funding Open access funding provided by Aalborg University. This work was supported by São Paulo Research Foundation (FAPESP # 21/07224–8), Conselho Nacional de Pesquisa (CNPq), Coordenação de Aperfeiçoamento de Pessoal de Nível Superior (CAPES), Carlsberg Foundation and INCT-Bioanalítica.

Data availability The datasets used in this work are available upon request.

Declarations

Conflict of interest The authors declare no conflict of interest.

Generative Ai and Ai-assisted technologies in the writing process The authors declare they did not use generative AI or AI-assisted technologies during the preparation of this work.

References

1. Fiore C, Rutherford T, Giuffrida F, Marmet C, Simone E. Crystallization behavior of plant-based fat blends formulated as an alternative for anhydrous milk fat in milk chocolate. Cryst Growth Des. 2025;25:2700–16. https://doi.org/10.1021/acs.cgd.5c00227.
2. Amasya G, Inal O, Sengel-Turk CT. SLN enriched hydrogels for dermal application: full factorial design study to estimate the relationship between composition and mechanical properties. Chem Phys Lipids. 2020;228:104889. https://doi.org/10.1016/j.chemphyslip.2020.104889.
3. Pinto F, de Barros DPC, Fonseca LP. Design of multifunctional nanostructured lipid carriers enriched with α-tocopherol using vegetable oils. Ind Crops Prod. 2018;118:149–59. https://doi.org/10.1016/j.indcrop.2018.03.042.
4. Guo Y, Song Z, Cao Y, Xiao J. Impact of cocoa butter and medium chain triglycerides ratios on processing stability, supersaturation, and digestive properties of curcumin-loaded nanostructured lipid carriers. LWT. 2024;1(197):115895. https://doi.org/10.1016/j.lwt.2024.115895.
5. Soddu E, Rassu G, Cossu M, Giunchedi P, Cerri G, Gavini E. The effect of formulative parameters on the size and physical stability of SLN based on "green" components. Pharm Dev Technol. 2016;21:98–107. https://doi.org/10.3109/10837450.2014.971376.
6. Ribeiro LNM, Breitkreitz MC, Guilherme VA, da Silva GHR, Couto VM, Castro SR, et al. Natural lipids-based NLC containing

lidocaine: from pre-formulation to *in vivo* studies. Eur J Pharm Sci. 2017;106:102–12. https://doi.org/10.1016/j.ejps.2017.05.060.
7. Intercontinental Exchange (ICE). ICE Futures U.S. Commodity and Indices Data – Cocoa. 2025. https://www.ice.com/report/292. Accessed on 19 Sep 2025.
8. Ghazani SM, Marangoni AG. Molecular origins of polymorphism in cocoa butter. Annu Rev Food Sci Technol. 2021;12:567–90. https://doi.org/10.1146/annurev-food-070620-022551.
9. Loke YH, Phang HC, Gobal G, Vijayaraj Kumar P, Kee PE, Widodo RT, et al. Application of cocoa butter for formulation of fast melt tablets containing memantine hydrochloride. Drug Dev Ind Pharm. 2024. https://doi.org/10.1080/03639045.2024.2417999.
10. Ray J, Smith KW, Bhaggan K, Stapley AGF. Crystallization and polymorphism of cocoa butter equivalents from blends of palm mid fraction and hard stearins produced by enzymatic acidolysis of high oleic sunflower oil. Eur J Lipid Sci Technol. 2022;124:2100228. https://doi.org/10.1002/ejlt.202100228.
11. Wille RL, Lutton ES. Polymorphism of cocoa butter. J Am Oil Chem Soc. 1966;43:491–6. https://doi.org/10.1007/BF02641273.
12. van Malssen K, van Langevelde A, Peschar R, Schenk H. Phase behavior and extended phase scheme of static cocoa butter investigated with real-time X-ray powder diffraction. J Am Oil Chem Soc. 1999;76:669–76. https://doi.org/10.1007/s11746-999-0158-4.
13. Loisel C, Keller G, Lecq G, Bourgaux C, Ollivon M. Phase transitions and polymorphism of cocoa butter. J Am Oil Chem Soc. 1998;75:425–39. https://doi.org/10.1007/s11746-998-0245-y.
14. Castro-Alayo EM, Balcázar-Zumaeta CR, Torrejón-Valqui L, Medina-Mendoza M, Cayo-Colca IS, Cárdenas-Toro FP. Effect of tempering and cocoa butter equivalents on crystallization kinetics, polymorphism, melting, and physical properties of dark chocolates. LWT. 2023;173:114402. https://doi.org/10.1016/j.lwt.2022.114402.
15. Bresson S, Rousseau D, Ghosh S, Marssi ME, Faivre V. Raman spectroscopy of the polymorphic forms and liquid state of cocoa butter. Eur J Lipid Sci Technol. 2011;113:992–1004. https://doi.org/10.1002/ejlt.201100088.
16. Reinke SK, Roth SV, Santoro G, Vieira J, Heinrich S, Palzer S. Tracking structural changes in lipid-based multicomponent food materials due to oil migration by microfocus small-angle X-ray scattering. ACS Appl Mater Interfaces. 2015;7:9929–36. https://doi.org/10.1021/acsami.5b02092.
17. MacMillan SD, Roberts KJ, Rossi A, Wells MA, Polgreen MC, Smith IH. In situ small angle X-ray scattering (SAXS) studies of polymorphism with the associated crystallization of cocoa butter fat using shearing conditions. Cryst Growth Des. 2002;2:221–6. https://doi.org/10.1021/cg0155649.
18. MacMillan SD, Roberts KJ, Wells MA, Polgreen MC, Smith IH. Identification of the initial nucleating form involved in the thermal processing of cocoa butter fat as examined using wide angle X-ray scattering (WAXS). Cryst Growth Des. 2003;3:117–9. https://doi.org/10.1021/cg025533t.
19. Teixeira CA, Poppi RJ. Discriminating blue ballpoint pens inks in questioned documents by Raman imaging and mean-field approach independent component analysis (MF-ICA). Microchem J. 2019;144:411–8. https://doi.org/10.1016/j.microc.2018.10.002.
20. Jouan-Rimbaud Bouveresse D, Rutledge DN. Independent Components Analysis: Theory and applications. In: Ruckebusch C, editor. Data Handling in Science and Technology. 2016. p. 225–77. https://doi.org/10.1016/B978-0-444-63638-6.00007-3
21. Galvão JG, Santos RL, Lira AAM, Kaminski R, Sarmento VH, Severino P, et al. Stearic acid, beeswax and Carnauba wax as green raw materials for the loading of carvacrol into nanostructured lipid carriers. Appl Sci. 2020;10:6267. https://doi.org/10.3390/APP10186267.
22. Kovačević AB, Müller RH, Keck CM. Formulation development of lipid nanoparticles: improved lipid screening and development of tacrolimus loaded nanostructured lipid carriers (NLC). Int J Pharm. 2020;576:118918. https://doi.org/10.1016/j.ijpharm.2019.118918.
23. Dang HS, Jannasch P. A comparative study of anion-exchange membranes tethered with different hetero-cycloaliphatic quaternary ammonium hydroxides. J Mater Chem A. 2017;5:21965–78. https://doi.org/10.1039/c7ta06029g.
24. Cardoso JF, Souloumiac A. Blind beamforming for non-Gaussian signals. IEE Proceedings, Part F: Radar and Signal Processing. 1993;140:362–70. https://doi.org/10.1049/ip-f-2.1993.0054.
25. Kassouf A, Jouan-Rimbaud Bouveresse D, Rutledge DN. Determination of the optimal number of components in independent components analysis. Talanta. 2018;179:538–45. https://doi.org/10.1016/j.talanta.2017.11.051.
26. Trevisan J, Angelov PP, Scott AD, Carmichael PL, Martin FL. IRootLab: A free and open-source MATLAB toolbox for vibrational biospectroscopy data analysis. Bioinformatics. 2013;29:1095–7. https://doi.org/10.1093/bioinformatics/btt084.
27. Ramel PR, Campos R, Marangoni AG. Effects of shear and cooling rate on the crystallization behavior and structure of cocoa butter: shear applied during the early stages of nucleation. Cryst Growth Des. 2018;18:1002–11. https://doi.org/10.1021/acs.cgd.7b01472.
28. Rigolle A, Goderis B, Van Den Abeele K, Foubert I. Isothermal crystallization behavior of cocoa butter at 17 and 20ºC with and without limonene. J Agric Food Chem. 2016;64:3405–16. https://doi.org/10.1021/acs.jafc.5b05965.
29. Hamley I. Diffuse scattering from lamellar structures. Soft Matter. 2022;18:711–21. https://doi.org/10.1039/d1sm01758f.
30. Hassanzadeh-Tabrizi SA. Precise calculation of crystalline size of nanomaterials: a review. J Alloys Compd. 2023;968:171914. https://doi.org/10.1016/j.jallcom.2023.171914.
31. Monakhova YB, Tsikin AM, Mushtakova SP, Mecozzi M. Independent component analysis and multivariate curve resolution to improve spectral interpretation of complex spectroscopic data sets: application to infrared spectra of marine organic matter aggregates. Microchem J. 2015;118:211–22. https://doi.org/10.1016/j.microc.2014.10.001.